INTERNATIONAL JOURNAL OF HYDROGEN ENERGY 44 (2019) 9529–9543

Available online at www.sciencedirect.com

ScienceDirect

journal homepage: www.elsevier.com/locate/he

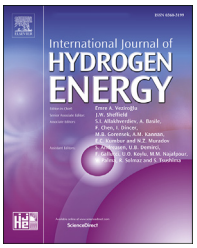

Trade-off designs and comparative exergy evaluation of solid-oxide electrolyzer based power-to-methane plants

Ligang Wang [a,b,*], *Johannes Düll* [c], *François Maréchal* [a], *Jan Van herle* [b]

[a] *Industrial Process and Energy Systems Engineering, École Polytechnique Fédérale de Lausanne (EPFL), 1951, Sion, Switzerland*

[b] *Group of Energy Materials, École Polytechnique Fédérale de Lausanne (EPFL), 1951, Sion, Switzerland*

[c] *Exergy Limited, The Design Hub, Technology Park, Puma Way, Coventry, CV1 2TT, United Kingdom*

ARTICLE INFO

Article history:
Received 12 May 2018
Received in revised form
30 October 2018
Accepted 19 November 2018
Available online 11 December 2018

Keywords:
Power-to-methane
Energy storage
Solid-oxide electrolyzer
Exergy analysis
Trade-off design

ABSTRACT

Solid-oxide electrolyzer (SOE) based power-to-methane (PtM) system can efficiently store surplus renewable power into synthesis natural gas by electrolysis and methanation. The system performance depends on the operating point of the electrolyzer and system design, particularly the heat exchanger network. In this paper, we investigate a SOE based PtM plant with a fixed-bed catalytic methanator and a membrane module for methane upgrading. A top-down approach is first employed to derive optimal system designs step by step from the system concept, to optimal conceptual designs with the trade-off between system efficiency and methane yield, to design-point selection and heat exchanger network design. Then, exergy evaluation with the exergy calculated into thermal – mechanical – non-reactive – reactive parts is applied to the derived four specific system designs to understand how exergy dissipation and performance of the overall system and each component vary from one to another. The results show that the system efficiency can reach between 80 and 85% (HHV) or 75–80% (LHV) when operating SOE with an inlet temperature of 700 °C and a utilization factor over 60%, above which electrical steam generation can be avoided and the steam can be generated by the heat from methanation reaction (around 80–85%) and anode outlet (15–18%). The system's exergy efficiency can achieve around 75–80% with the input exergy mainly destructed within the SOE (25–35%), methanator (25–35%) and heat exchangers (10–17%). However, exergy efficiencies of the SOE and methanator are high, over 90%. Depending on the temperature level of the cold stream and the temperature difference, heat exchangers generally have an exergy efficiency of over 50–80%. The electrical steam generator can only achieve an efficiency of around 20% and leads to a significant drop of system efficiency if employed; however, small electrical heating to reach the desired SOE inlet temperature, although bad, is acceptable. Therefore, one preliminary design guideline for such systems should be the avoidance of electrical steam generation.

* *Corresponding author*. Group of Energy Materials, École Polytechnique Fédérale de Lausanne, 1951, Sion, Switzerland.
E-mail addresses: lgwangeao@163.com, ligang.wang@epfl.ch (L. Wang).

https://doi.org/10.1016/j.ijhydene.2018.11.151

Introduction

The share of renewable energy sources (RES) for the European power-generation sector has already reached almost 30%, and for some countries, such as Denmark, Latvia, Austria, Portugal and Sweden, the RES share for power generation has been over 50% [1]. In the heating and cooling sectors, however, only about 20% comes from RES; and in the transport sector the 7% mark was just exceeded in 2016 [3]. With this increased use of variable renewable energy sources (VRES) in the past decade [2], the share of RES in European gross final energy consumption has been expected as 27% in 2030 [3].

To enable higher RES penetration, a further development of relevant infrastructure is the way forward for future energy systems [1,4]. Many strategies and technologies are being applied and developed, such as demand-side management, balancing and reserving power sources, power-grid expansion, cross-border interconnectivity, short-term storage (e.g., Pb-acid, molten-salt and Li-ion batteries) and long-term storage (e.g., pumped hydro storage and compressed air energy storage [5,6]) [7,8]. As a new integral and promising approach, power-to-x (PtX) technologies have attracted more and more attention [9], since they not only serve for demand-side management and energy storage but also facilitate the substitution of fossil fuels in the sectors of building, industry and transport. PtX technologies can convert surplus renewable power to various energy forms or chemical substances, e.g., thermal energy (power-to-heat), liquids (power-to-liquid), hydrogen or methane (power-to-gas (PtG)) or other chemicals (power-to-chemicals), such as solvents, formic acid, alcohols and waxes [10].

Power-to-methane (PtM), which converts renewable power first into H_2 (or syngas) through the electrolysis of water/steam (or together with CO_2) and then into synthesized natural gas (SNG) via methanation processes, is particularly attractive, due to (1) the cheap and large-scale capacity of methane storage offered by existing gas-grid infrastructure [11–13], (2) the frequent use of natural gas at district and household level for heating or co-generation, and (3) the substitution of diesel and petrol in the transport sector by natural-gas mobility with sufficient performance [10,14]. Although short-haul and public transport could be transferred to electromobility in the mid-term, it is still limited by insufficiently-dimensioned infrastructure and the lack of mass production [9,15].

Power-to-methane based on low-temperature electrolysis continues to be known for high capital costs and low round-trip efficiencies [16,17]. Thanks to the emerging high-temperature solid-oxide electrolyzer (SOE) with high electrical efficiency, the PtM system efficiency is expected to be largely increased at potentially lower costs [18], especially due to plant-wise heat integration: the methanation heat can be used to generate steam for the SOE. The first SOE-based PtM demonstrator with such thermal integration [19,20] was expected to achieve an system efficiency of 76%, about 15–25 percentage points higher than that of the PtM plants based on low-temperature electrolysis [16,21,22]. Similar concept has been applied for biogas upgrading in Denmark [23] by injecting H_2 generated from the SOE to cleaned biogas ($CH_4 + CO_2$) and converting CO_2 to CH_4 in a subsequent catalytic methanator, which generates part of the steam for the SOE. Also, for the small-scale SOE based PtM plant to be demonstrated in PENTAGON project [24] aiming at increasing the energy storage capability at local district level, the coupling between the SOE and the methanator will be achieved by an intermediate heat-transfer fluid, thermal oil, which carries methanation heat to the steam generator. Although all these demonstrations have not put the SOE-methanator coupling into operation up to now, it has been recognized widely as the most effective measure to improve the PtM performance.

The performance of SOE-based PtM can be improved by varying operating points of the SOE and plant-wise heat integration [25,26]. To understand how the system performance is improved from one design to another, component-based exergy analysis can be employed, which identifies the sources and magnitudes of the thermodynamic inefficiencies occurring with each component, highlights the components with the highest inefficiencies, and pinpoints the directions for system improvement [27]. Exergy analysis has been employed to examine various thermal systems, e.g., thermal power plants [28–31], vapor compression refrigeration systems [32], drying processes and systems [33] and renewable energy systems [34,35]. However, there have been only limited applications to the SOE-based systems. For power-to-hydrogen, the effects of operating variables on the system's exergetic efficiency have been investigated in Refs. [36,37], which illustrated contradictory trends: For a fixed plant layout, an increase in current density above 800 °C resulted in an exergy-efficiency decrease in Ref. [36] but an increase in Ref. [37]. Similar work done in Ref. [38] for a given power-to-syngas system with SOE operating at 800 °C and fixed flowrates of feedstock and air concluded a maximum exergy efficiency of 60% achieved at a feedstock conversion of 64%, which is significantly lower than the state-of-the-art. For PtM, the optimal operating conditions to maximize exergy efficiency were investigated in Ref. [22] for a system with fixed system layout and CO_2 removal to upgrade methane; however, the concluded operating points with the highest exergy efficiency may not be appropriate, since the current density was varied without adapting the H/C feed ratio, or vice versa. In practice, these two variables should be changed simultaneously to produce syngas with its composition suitable for methanation, $(H_2 - CO_2)/(CO + CO_2) = 3$. The major problems of these published work are:

- The analyzed system is with only one specific system layout, which is not adapted to maximize the benefit of varying design variables.
- The exergy of a stream is split only to physical and chemical exergy, which may result in inappropriate definition of exergy efficiency of a component.
- Component-based analysis is not detailed discussed to focus on how input exergy is destructed along energy conversion and transfer inside the system.

Therefore, the two major innovations of this paper are summarized:

- System designs with the optimal design variables and their corresponding system layouts derived from a top-down

approach. Optimal design points with the trade-off between system efficiency and methane yield are realized with specific heat exchanger networks derived from heat cascade utilization.
- In-depth component-based exergy evaluation by splitting exergy flows into thermal – mechanical – nonreactive – reactive parts and with an accurate definition of exergy efficiency at the component level.

The paper is organized as following: In Description and technology specification of the SOE-based power-to-methane plan, system designs are provided step by step from the system concept (Concept of the small-scale power-to-methane demonstration), to trade-off conceptual designs and design-point selection (Optimal conceptual design for design-point selection), to specific system designs and layouts with heat exchanger networks (Heat exchanger network of the selected conceptual designs). In Exergy analysis, exergy analysis including exergy calculation exergy balance at both component and system levels is first introduced in Exergy analysis methodology and then implemented to the proposed systems in Implementation. Then, in Results and discussion, the overall system performance, the exergy-dissipation distribution and the exergy efficiency of each component are comparatively discussed. Finally, the conclusion is drawn in Conclusions.

Description and technology specification of the SOE-based power-to-methane plant

The SOE-based PtM system under demonstration of EU H2020 project PENTAGON [24] is targeting energy storage capability at local district level to enhance the flexibility of local grid operation with high penetration of renewable energies. Practical system efficiency of the plant is expected to be at around 70–75% (higher heating value, HHV) with a cathode-supported SOE stack (64 plate cells × 80 cm^2).

Concept of the small-scale power-to-methane demonstration

The schematic of the considered SOE-based PtM system is given in Fig. 1, without specific heat exchanger networks (HEN), auxiliary components and gas-recirculation devices explicitly illustrated. The processed, demineralized water (1) is vaporized and mixed with the re-circulated gas (6a) to provide 10 vol% H_2 for cathode (the H_2 evolution electrode) to avoid the re-oxidation of the Ni-YSZ electrode and support [39–41]. The mixed feed (2) is further heated up to the desired temperature (700 °C considered in this paper) either completely by SOE outlets or partially by electrical heating, depending on the SOE operating points. The fed steam (2a) is partially split into H_2, which is further cooled down in a flash drum for water knock-out (1c). To remove the O_2 generated at the anode, sweep air (3) is usually fed to the SOE at the same temperature as the steam feed, which can carry certain heat into or out of the stack. In principle, the SOE can also operate with pure oxygen production with a different design of the anode-related subsystem: The air heater and blower at the anode inlet are no longer needed; instead, an induced draft fan will be equipped at the anode outlet.

For the methanation sub-process, the dry product from the SOE (6b,6c) and pre-heated CO_2 (7a) are first mixed with the recirculated, cooled unreacted gas (11a) and then heated up to around 220–240 °C (8a) before entering the fixed-bed catalytic reactor, which is assumed to operate isothermally at 280 °C (the optimal temperature range for various catalysts reported in elsewhere, e.g. [19,20]). The methanation heat can be effectively extracted by steam generation internally in the reactor to keep the reactor temperature within a preferred range. The steam produced can be further heated and sent to the SOE. The gas mixture out of the reactor (9) is cooled down with water knock-out (1f). Then, the dry gas mixture (10) enters the membrane module to obtain high-purity methane (12, over 96 vol%) for grid injection. The permeate unreacted gas of the membrane (11) is then recycled back and mixed with initial feeds to the methanation process. Note that for CO_2 methanation reaction, the CO_2 molar feed of the stream 7a is specified around a quarter of the molar feed of H_2 in stream 6c. Given the situation that only small amount unreacted gases are recycled via 11a, the H/C ratio of the stream 8 and 8a is close to 8, which does not lead to the risk of carbon decomposition at the catalyst surface.

This concept is particularly suitable for small-scale applications, due to the scalability of the membrane module for CH_4 upgrading. However, it can be adapted readily for large-scale applications by employing other concepts of methanation process, e.g., a series of methanation reactors. The system is with a SOE stack of 64 cells with 80 cm^2 active area. Other system components are sized based on the operating points of the SOE and the methanator.

Optimal conceptual design for design-point selection

To support the selection of design points, the system performance is predicted with calibrated component models, optimized and analyzed by a multi-objective optimization platform with mathematically-formulated heat-cascade calculation [25]. The key models involved are:

- The quasi-2D SOE model described in Ref. [25] and employed in this paper considers electrochemistry, mass and heat transfer, reaction kinetics and chemical equilibrium, and has been calibrated with the multiple test data for both cell and stack. The model can accurately predict the SOE performances under various operating conditions.
- The methanator performance is calculated by chemical equilibrium under isothermal conditions, to be achieved in practice. The methanator concepts with internal steam generation at elevated pressure have been investigated in Refs. [19,42] to achieve evenly-distributed temperature in the reaction zone within the preferred range.
- The 1D membrane model described in Ref. [25] can work with different options of flow directions, e.g., co-flow, counter-flow or cross-flow. For separating CH_4 from CH_4/H_2/CO_2 mixture, polyimide membrane [43] is used with the permeability (barrier) at 30 °C: H_2 28.1, N_2 0.32, O_2 2.13, CH_4 0.25, CO_2 10.7.

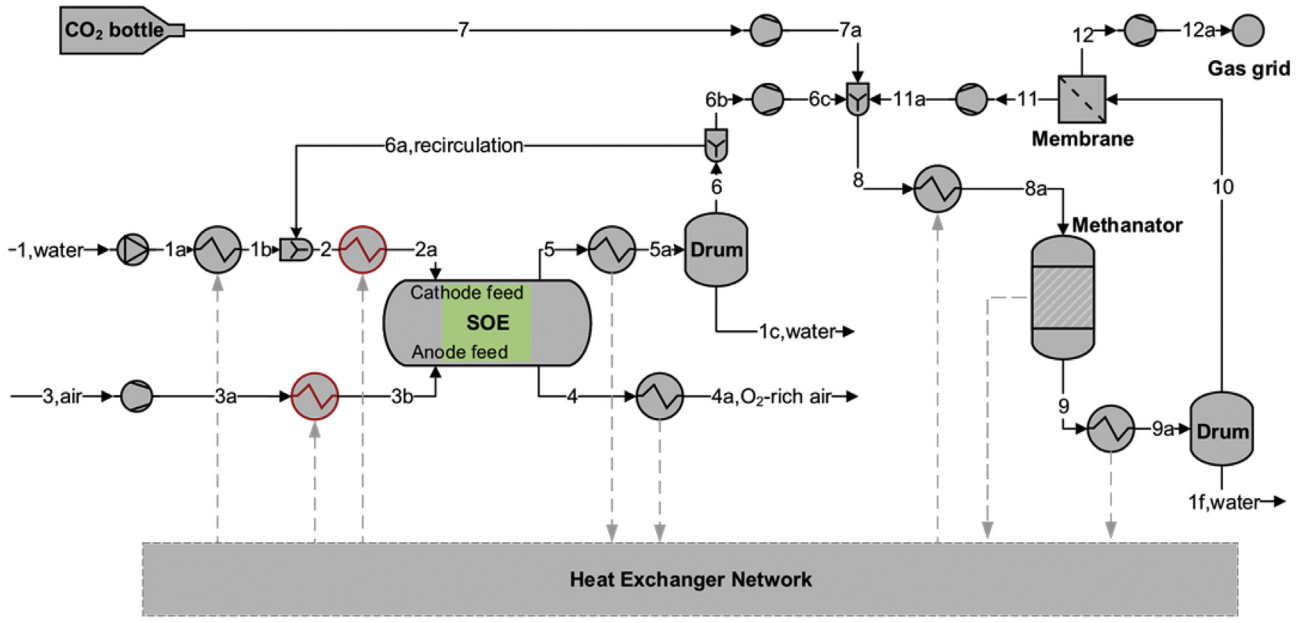

Fig. 1 – Concept of the SOE-based PtM plant with the SOE operating under steam electrolysis mode (no explicit HEN and components for start-up, hot stand-by and gas recirculation illustrated, adapted from Refs. [25,26]. The heaters in red may be partially driven by electrical heating to heat up the anode/cathode feeds to the expected temperatures). (For interpretation of the references to colour in this figure legend, the reader is referred to the Web version of this article.)

The system performance is optimized in terms of methane yield and system efficiency, which is defined as:

$$\eta_{HHV} = \dot{m}_{CH_4} HHV / \dot{E}_{TOT} \quad (1)$$

where the total power consumption $\dot{E}_{tot}$ is contributed by the electrolyzer, electrical heaters, fans, compressors and pumps.

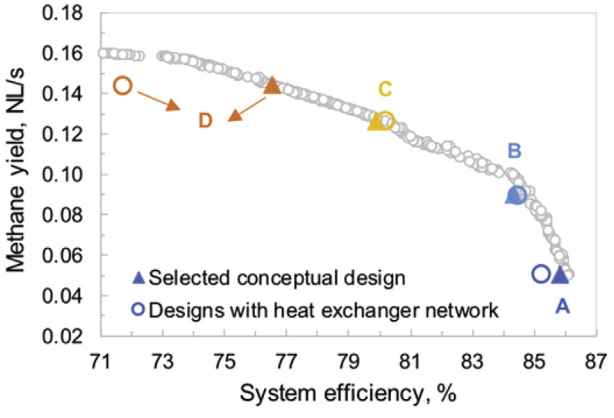

Fig. 2 – The Pareto front obtained with the SOE operating under steam-electrolysis mode and an inlet temperature of 700 °C (recalculated based on [25]) with the selected conceptual designs and specific designs with heat exchanger network from Heat exchanger network of the selected conceptual designs. Additional information on the Pareto solutions is given in Fig. S1. For more comprehensive understanding of the Pareto front, the reader is referred to [25].

The optimization considers the following key operating parameters with practical bounds:

- For SOE, operating pressure (p_{SOE}, 1.1–30 bar), steam utilization factor (*UF*, 50–80%), steam flowrate ($\dot{F}_{stm}$, 2.5–25 standard cubic centimeters per minute per cm^2 (sccm/cm^2)), and sweep-air feed flowrate ($\dot{F}_{air}$, 0–30 sccm/cm^2). With zero sweep-air feed, the SOE is operated with pure oxygen production.
- For methanator, operating pressure p_{METH} (1.1–30 bar)
- For membrane, permeate pressure p_{PERM} (0.5–15 bar)

The optimization is performed with an inlet temperature of the stack 700 °C, a maximum temperature difference inside the stack of 120 °C, methanation temperature of 290 °C, and a gas-grid pressure of 85 bar. Although the gas-grid pressure depends on the country and the type of methane distribution network, it does not lead to big influence on the optimal solutions identified.

The key outcome from the bi-objective optimization is a Pareto front, which illustrates the trade-off between the two selected objective functions, i.e., methane yield and system efficiency (HHV). Each solution on a Pareto front, namely Pareto-optimal solution, represents the solution achieving the maximum methane production for a given system efficiency. The Pareto solutions identified are with different operating points of the components and plant-wise heat integration. If a system is not optimally designed, the methane yield is always lower than the Pareto solution with the same system efficiency. Therefore, practical, feasible region of system design is on and below the Pareto front. It

has been found in Ref. [25] that, for a given SOE hardware, pursuing higher system efficiency reduces the maximum methane production, as shown in Fig. 2. If methane yield is expected to be increased, the current density and steam feed need to be enlarged as shown in Figure S 1: (1) The increase in current density leads to an increased voltage (overpotential), which decreases electrolysis (electrical) efficiency and thus system efficiency, since electrolysis power dominates the total power. (2) The increase in steam feed reduces steam utilization factor, thus worsening the plant-wise heat integration, since the bottleneck of heat utilization is water vaporization.

Four Pareto-optimal conceptual designs with different system performances are selected for further designs (Fig. 2). The four designs are chosen approximately evenly distributed on the Pareto front with different operating current density. It should be noted that, when selecting the design points, the effect of the current density on performance degradation of the electrolyzer is not considered, since many conditions of the identified Pareto solutions, particularly at high the current density, have not been tested yet in any experiment. Therefore, the study presented here can also link the experimental designs with the identified operating conditions to test the corresponding stack durability.

The features of the four conceptual designs are summarized as follows and key operating variables are listed in Table 1:

- Conceptual design A: the highest efficiency, (close to) pure oxygen production, elevated pressure
- Conceptual design B: (close to) pure oxygen production, elevated pressure
- Conceptual design C: sweep air, atmospheric pressure
- Conceptual design D: large methane yield, sweep air, atmospheric pressure

Heat exchanger network of the selected conceptual designs

With the identified optimal operating points, HENs of each conceptual design are then specifically designed based on the heat cascade utilization and considering network complexity. For the proposed system, special guidelines for the HEN design are:

- Cathode outlet is used to heat cathode inlet. Due to the smaller heat capacity of cathode outlet, the heat carried by cathode outlet is usually not enough to heat cathode inlet up to 700 °C, thus electrical heating may be needed.
- Anode outlet is used to heat anode inlet. Due to the higher heat capacity of anode outlet caused by the increased oxygen content, there is usually additional heat available after heating the anode inlet up to 700 °C, which can be used for steam generation.
- Steam can be generated by the methanator, anode outlet, and electrical heating (if needed).
- For the methanator design, the inlet gas can be heated inside the reactor, if properly designed.

With these considerations, the common, complete flowsheet for all the four conceptual designs is illustrated in Fig. 3, where some components are only needed for certain designs. Detailed flowsheets, key information of HEN and stream data for each conceptual design are given in Figs S2–S5, Tables S1–S8, respectively.

Exergy analysis

Exergy analysis methodology

Exergy analysis considers not only the quantity but also the quality of energy flows, and is beneficial to understand the spatial dissipation of exergy inside an energy system [44], which helps to propose means of improving the system's performance [45].

Exergy of material flows

The total exergy E^{TO} of a material stream k includes physical (E^{PH}) and chemical (E^{CH}) exergies. Physical exergy is defined as the maximum theoretical useful work obtainable by bringing the stream to the temperature (thermal effect) and pressure (mechanical effect) of thermodynamic reference environment by an ideal process without changing its chemical composition:

$$E_k^{PH} = E_k^{TH} + E_k^{ME} = E_k(T,\ p,\ x \rightarrow T_0,\ p_0, x) \quad (2)$$

where $H_{0,k}$ and $S_{0,k}$ represent the enthalpy and entropy of the stream k under the reference states (for this paper, $T_0 = 25$ °C

Table 1 – Technical specifications of the components of the selected design points and key performance indicators of the system with SOE inlet temperature of 700 °C.

	Key specifications with related stream number given in Fig. 1									Key performance indicators				
	p_{2a}	T_5	$\dot{F}_1$	$\dot{F}_{2a}$	$\dot{F}_{3b}$	V_{cell}	J_{cell}	p_{8a}	p_{11}	UF	$\dot{W}_{SOE}$	$\dot{W}_{tot}$	$\dot{F}_{CH_4,12}$	$y_{CH_4,12}$
	bar	°C	sccm/cm^2	sccm/cm^2	sccm/cm^2	V	A/cm^2	bar	bar	%	kW	kW	NL/s	%
A	26.0	740	2.88	3.35	0.12[a]	1.30	0.34	26	4.7	80	2.3	2.3	0.050	96.2
B	9.70	809	5.25	6.10	0.26[a]	1.32	0.61	10	3.8	78	4.1	4.2	0.090	96.5
C	1.12	819	9.26	10.8	7.83	1.36	0.86	6.0	1.9	62	6.0	6.3	0.126	96.4
D	1.18	819	11.9	14.0	24.4	1.42	0.98	7.9	4.8	55	7.1	7.5	0.144	96.4

[a] The sweep-air flowrates for the design A and B are set as 0 when designing detailed HEN in Heat exchanger network of the selected conceptual designs. This is due to that the small sweep-air flowrates lead to very small air-air heat exchangers. The resulting designs A and B in Heat exchanger network of the selected conceptual designs are with pure O_2 production.

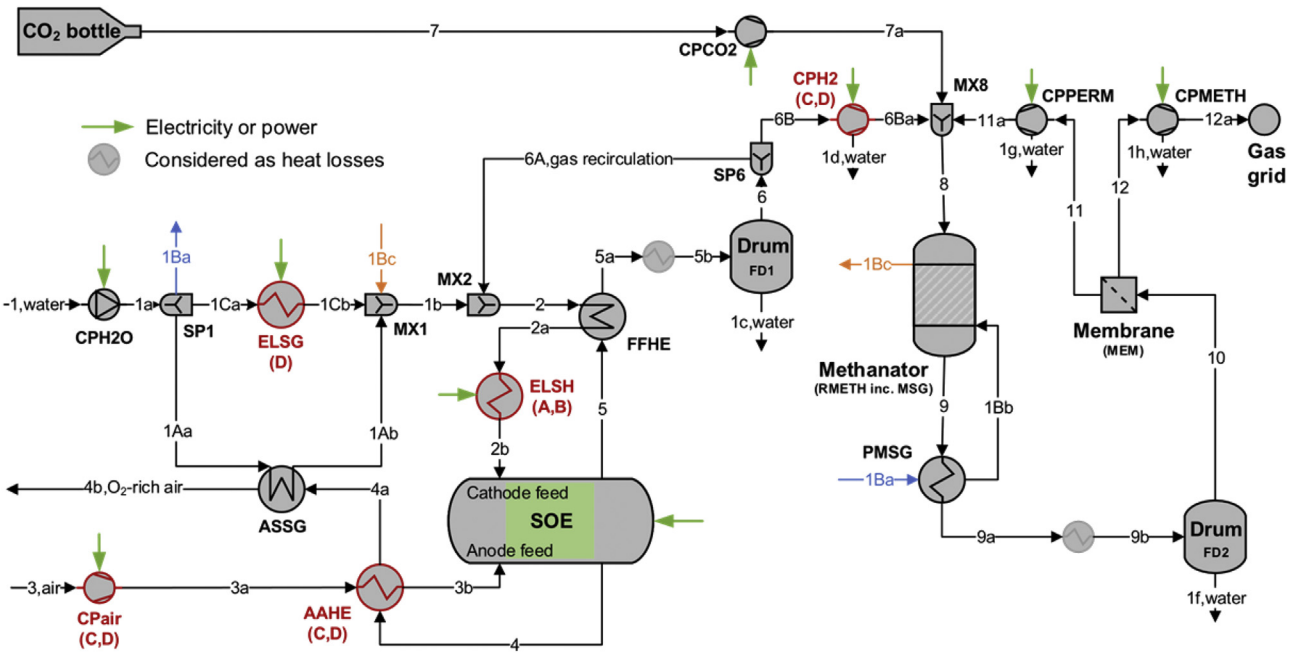

Fig. 3 – Heat exchanger network design for the selected four conceptual designs. The red-colored components are only used for the indicated designs, e.g., ELSG only for the design D, ELSH only for the designs A and B. Stream 1Ba from SP1 flows to PMSG and stream 1Bc comes from RMETH. AAHE: air-air heat exchanger; ASSG: air-side steam generator; ELSG: electrical steam generator; FFHE: fuel-fuel heat exchanger; ELSH: electrical superheater; RMETH: methanator; MSG: main steam generator included in RMETH; PMSG: water preheater of main steam generator. Complete flowsheets and additional information are given in supporting information. (For interpretation of the references to colour in this figure legend, the reader is referred to the Web version of this article.)

and $p_0 = 1$ atm) with its original chemical composition $\mathbf{x}$. The thermal (E_k^{TH}) and mechanical (E_k^{ME}) exergies are employed to evaluate the processes of heat integration and compression/expansion related to the considered stream k:

$$E_k^{TH} = E(T, p, \mathbf{x} \rightarrow T_0, p, \mathbf{x}) = (H_k - H_{T_0,p,x,k}) - T_0(S_k - S_{T_0,p,x,k}) \quad (3)$$

$$E_k^{ME} = E(T_0, p, \mathbf{x} \rightarrow T_0, p_0, \mathbf{x}) = (H_{T_0,p,x,k} - H_{T_0,p_0,x,k}) - T_0(S_{T_0,p,x,k} - S_{T_0,p_0,x,k}) \quad (4)$$

The chemical exergy of a mixture is defined as the useful work obtainable by converting the substances of the considered mixture k to the compositions of the thermodynamic reference environment via ideal mixing and separation, and chemical reactions, which are corresponding non-reactive exergy (E^N) and reactive exergy (E^R). Such a splitting of chemical exergy enables to consider the effects that are related to the changes in composition ("excess exergy"), and chemical reactions [46]. The reactive exergy is represented by the standard chemical exergies of each chemical substance i ($\bar{e}_i^{CH}$). The chemical exergy of a gas mixture is calculated based on [47]:

$$E_k^{CH} = E_k^N + E_k^R = E_k(T_0, p_0, \mathbf{x} \rightarrow T_0, p_0, \mathbf{x}_0) = \dot{n}\left(\sum_i x_i e_i^{-CH} + RT_0 \sum_i x_i \ln(x_i)\right) \quad (5)$$

$$E_k^N = \sum_i x_i E_i(T_0, p_0, \mathbf{x} \rightarrow T_0, p_0, x_i = 1) = \dot{n}\sum_i^N x_i R T_0 \ln(x_i) \quad (6)$$

$$E_k^R = \sum_i x_i E_i(T_0, p_0, x_i = 1 \rightarrow T_0, p_0, x_0) = \dot{n}\sum_i^N x_i e_i^{-CH} \quad (7)$$

where x and $\dot{n}$ stand for the molar fraction and flowrate, and R is the ideal gas constant. The standard chemical exergies of pure substances involved in the proposed system are taken from [48]: CH_4 (g) 832.00 kJ/mol, CO (g) 274.71 kJ/mol, CO_2 (g) 19.48 kJ/mol, H_2 (g) 236.09 kJ/mol, H_2O (l) 0.90 kJ/mol, N_2 (g) 0.72 kJ/mol and O_2 (g) 3.97 kJ/mol.

It occurs frequently for a gas mixture with water that the liquid fraction may vary when changing the mixture state to p_0 and T_0. In such a case, the chemical exergy is calculated based on gas- and liquid-phase composition ($\mathbf{x} = \mathbf{x}^g + \mathbf{x}^l$) at p_0 and T_0 as follows [47]:

$$E_k^{CH} = \dot{n}\left(\sum_i x_i^g e_i^{-CH,g} + RT_0 \sum_i x_i^g \ln(x_i^g) + \sum_i x_i^l e_i^{-CH,l}\right) \quad (8)$$

where $\bar{e}_i^{CH,g}$ and $\bar{e}_i^{CH,l}$ are the standard chemical exergy of gas and liquid phase of substance i.

Component-based exergy analysis

(1) Component level

At the component level, the exergy balance of a component j is defined as:

$$\dot{E}_{F,j} = \dot{E}_{P,j} + \dot{E}_{D,j} + \dot{E}_{C,j} \quad (9)$$

where exergy fuel (F) and product (P) of the component j are determined following the methodology described in [49]. The exergy product of a component represents the useful and desired effect it delivers, whereas the exergy fuel represents the amount of exergy consumed by the same component to generate the product. Usually, it is considered that the difference between the exergy fuel and product of a component is defined as exergy destruction ($\dot{E}_D$) of the component; however, to achieve the productive purpose, some additional effects, which may not be expected but are necessary due to thermodynamics, may occur. For example, the purpose of a gas compressor is to increase the mechanical exergy of the gas, but gas compression leads to an increase in its outlet temperature by consuming part of the power consumed. These co-productive effects sometimes can be useful to the downstream. We consider these additional effects in a separate term, $\dot{E}_C$ (the co-product), which should be always larger than 0 (otherwise, it is a part of the exergy fuel). Note that it is not always necessary to distinguish the productive and co-productive effects, since the difference may be minor.

For the productive exergy efficiency of a component as mostly discussed in literature, there have been several definitions based on, e.g., inlet – outlet flows of total exergies, or exergy fuel and product. The latter has been widely accepted:

$$\varepsilon_j^P = \frac{\dot{E}_{P,j}}{\dot{E}_{F,j}} = 1 - \frac{\dot{E}_{D,j} + \dot{E}_{C,j}}{\dot{E}_{F,j}} \quad (10)$$

Considering the co-productive effects caused by thermodynamics, we can also define a thermodynamic exergy efficiency, which assumes that the co-productive effects occurring in one component are helpful for and the related exergy $\dot{E}_C$ can be used by its connected downstream components:

$$\varepsilon_j^T = \frac{\dot{E}_{P,j} + \dot{E}_{C,j}}{\dot{E}_{F,j}} = 1 - \frac{\dot{E}_{D,j}}{\dot{E}_{F,j}} \quad (11)$$

(2) System level

At the system level, exergy flows can leave a system as losses without a productive purpose and linked to the interaction of the system with the thermodynamic reference environment via material or heat/power flows:

$$\dot{E}_{F,SYS} = \dot{E}_{P,SYS} + \dot{E}_{D,SYS} + \dot{E}_{L,SYS} = \dot{E}_{P,SYS} + \sum_j \dot{E}_{D,j} + \dot{E}_{L,SYS} \quad (12)$$

The (productive) exergy efficiency of the system therefore can be defined as:

$$\varepsilon_{SYS} = \frac{\dot{E}_{P,SYS}}{\dot{E}_{F,SYS}} = 1 - \frac{\dot{E}_{D,SYS} + \dot{E}_{L,SYS}}{\dot{E}_{F,SYS}} \quad (13)$$

The "thermodynamic" exergy efficiency for the system level is not meaningful, since utilizing the exergy lost from the system, e.g., by waste heat recovery from the outlet gas streams, is not part of the system and depends on the specific technology.

Implementation

The exergy destruction of a component is independent from the definitions of exergy fuel and product. However, exergy efficiency relies on accurate and meaningful definitions of exergy fuel and product. With the splitting of the exergy flow into thermal – mechanical – non-reactive – reactive exergy (TMNR system), the exergy fuel, product as well efficiency can be accurately (or simply reasonably) defined, which sometimes can be achieved by using a physical – chemical exergy (PC) system or an inlet – outlet (IO) system, especially for electro-chemical devices and multi-purpose reactors. In the following, we give the definitions of exergy fuel, product and coproduct for each component based on TMNR, PC and IO (inlet – outlet) systems.

For the TMNR and PC approaches, the definitions of exergy fuel, product and co-product are listed in Tables 2 and 3, respectively. The formulations for the splitters, SP1 and SP6, are not listed, since the exergy efficiency is always 100% for this study. The formulations for the compressors, CPH2, CPCO2 and CPPERM are also not listed, which are similar to that of CPAIR. The major differences between the two definition approaches come from the (electro-)chemical reactor (RMETH and SOE) and gas separation units (MEM). With TMNR approach, the exergy fuel, product and co-product of RMETH, SOE and MEM can be described as:

- RMETH
  - o Exergy fuel: the chemical exergy of the reactant (H_2/CO_2)
  - o Exergy product: (1) the chemical exergy of newly-generated methane and (2) the increment of thermal exergy of water/steam
  - o Exergy co-product: the increment of physical exergy of the reacting flow
- SOE (for exothermic operation)
  - o Exergy fuel: power consumed
  - o Exergy product: the chemical exergy of the newly-generated hydrogen
  - o Exergy co-product: (1) the increment of total exergy of sweep gas and (2) the increment of the exergy of cathode flow excluding the chemical exergy of hydrogen
- MEM
  - o Exergy fuel: the decrement of mechanical exergy
  - o Exergy product: the increment of non-reactive exergy

The TMNR and PC splitting of the exergy of each stream has been shown in Tables S2,S4,S6 and S8 for design A, B, C, D, respectively.

For the IO approach, the exergy efficiency of the considered component j can be straightforward defined as

$$\varepsilon_{IO,j} = \frac{\sum_k^{N_{out}} \dot{E}_k^{TO}}{\sum_k^{N_{in}} \dot{E}_k^{TO}} \quad (14)$$

Table 2 – Definitions of exergy fuel, product and co-product of each component based on TMNR exergy splitting[a]. Some zero terms are neglected in the table.

Comp.	Fuel	Product	Co-product
CPH2O[b]	$\dot{W}_{CPH2O}$	$\dot{E}_{1a}^{ME} - \dot{E}_{1}^{ME}$	–
CPAIR[b]	$\dot{W}_{CPAIR}$	$\dot{E}_{3a}^{ME} - \dot{E}_{3}^{ME} + \dot{E}_{out,N_{final}}^{TH} - \dot{E}_{in,N_{final}}^{TH}$	$\sum_{i}^{N_{stage}-1} \dot{E}_{out,i}^{TH} - \dot{E}_{in,i}^{TH}$
CPMETH[b]	$\dot{W}_{CPMETH}$	$\dot{E}_{12a}^{ME} - \dot{E}_{12}^{ME}$	$\sum_{i}^{N_{stage}} \dot{E}_{out,i}^{TH} - \dot{E}_{in,i}^{TH}$
AAHE	$\dot{E}_{4}^{TH} - \dot{E}_{4a}^{TH}$	$\dot{E}_{3b}^{TH} - \dot{E}_{3a}^{TH}$	–
ASSG	$\dot{E}_{4a}^{TH} - \dot{E}_{4b}^{TH}$	$\dot{E}_{1Ab}^{TH} - \dot{E}_{1Aa}^{TH}$	–
PMSG	$\dot{E}_{9}^{TH} - \dot{E}_{9a}^{TH}$	$\dot{E}_{1Bb}^{TH} - \dot{E}_{1Ba}^{TH}$	–
FFHE	$\dot{E}_{5}^{TH} - \dot{E}_{5a}^{TH}$	$\dot{E}_{2a}^{TH} - \dot{E}_{2}^{TH}$	–
ELSG	$\dot{W}_{ELSG}$	$\dot{E}_{1Cb}^{TH} - \dot{E}_{1Ca}^{TH}$	–
ELSH	$\dot{W}_{ELSH}$	$\dot{E}_{2b}^{TH} - \dot{E}_{2a}^{TH}$	–
MX2	$\dot{E}_{6A}^{TO} + \dot{E}_{1b}^{TO}$	$\dot{E}_{2}^{TO}$	–
MX8	$\dot{E}_{7a}^{TO} + \dot{E}_{6Ba}^{TO} + \dot{E}_{11a}^{TO}$	$\dot{E}_{8}^{TO}$	–
RMETH (inc. MSG)	$(\dot{E}_{8}^{CH} - \dot{E}_{8}^{R,CH_4}) - (\dot{E}_{9}^{CH} - \dot{E}_{9}^{R,CH_4}) + (\dot{E}_{1Bb}^{ME} - \dot{E}_{1Bc}^{ME})$	$(\dot{E}_{9}^{R,CH_4} - \dot{E}_{8}^{R,CH_4}) + (\dot{E}_{1Bc}^{TH} - \dot{E}_{1Bb}^{TH})$	$(\dot{E}_{9}^{PH} - \dot{E}_{8}^{PH})$
SOE[c]	$\dot{W}_{SOE}$	$\dot{E}_{5}^{R,H_2} - \dot{E}_{2b}^{R,H_2}$	$(\dot{E}_{4}^{TO} + (\dot{E}_{5}^{TO} - \dot{E}_{5}^{R,H_2})) - (\dot{E}_{3b}^{TO} + \dot{E}_{2b}^{TO} - \dot{E}_{2b}^{R,H_2})$
MEM[d]	$\dot{E}_{10}^{ME} - (\dot{E}_{11}^{ME} + \dot{E}_{12}^{ME})$	$\dot{E}_{11}^{N} + \dot{E}_{12}^{N} - \dot{E}_{10}^{N}$	–

[a] The stream numbers given here are based on Fig. 3 but might be different from design A to D. For the specific designs, refer the stream numbers according to Figs. S2–S5.

[b] The TMNR definition of CPMETH is different from those of CPH2O and CPAIR (CPH2, CPCO2 and CPPERM), which are connected to subsequent heating processes. The increase in thermal exergy at the outlet of the five pumps or compressors is expected, while for the grid injection, thermal exergy of the stream 12a is not expected. Note that, for compressors, this detailed splitting does not cause large difference to the exergy efficiency.

[c] The definitions of the SOE depends on the operating point. For exothermic operation (the case for this paper), the thermal exergy increase between inlet and outlet is counted as co-product, while for endothermic operation, the thermal exergy decrease between inlet and outlet will be counted as exergy fuel.

[d] The exergy product of the membrane, $\dot{E}_{11}^{N} + \dot{E}_{12}^{N} - \dot{E}_{10}^{N}$. is almost equal to $(\dot{E}_{11}^{T} - \dot{E}_{11}^{ME}) + (\dot{E}_{12}^{T} - \dot{E}_{12}^{ME}) - (\dot{E}_{10}^{T} - \dot{E}_{10}^{ME})$.

Table 3 – Definitions of exergy fuel, product and co-product of pumps, compressors, RMETH, SOE and MEM based on PC exergy splitting[a]. The definitions for the other components (heat exchangers and mixers) are the same to those given in Table 2 by replacing thermal exergy with physical exergy.

Comp.	Fuel	Product	Co-product
CPH2O	$\dot{W}_{CPH2O}$	$\dot{E}^{PH}_{1a} - \dot{E}^{PH}_{1}$	–
CPAIR	$\dot{W}_{CPAIR}$	$\dot{E}^{PH}_{3a} - \dot{E}^{PH}_{3}$	–
CPMETH	$\dot{W}_{CPMETH}$	$\dot{E}^{PH}_{12a} - \dot{E}^{PH}_{12}$	–
RMETH (inc. MSG)	$\dot{E}^{CH}_{8}$	$\dot{E}^{CH}_{9} + (\dot{E}^{PH}_{1Bc} - \dot{E}^{PH}_{1Bb})$	$(\dot{E}^{PH}_{9} - \dot{E}^{PH}_{8})$
SOE[b]	$\dot{W}_{SOE}$	$\dot{E}^{CH}_{5} - \dot{E}^{CH}_{2b}$	$(\dot{E}^{TO}_{4} + \dot{E}^{PH}_{5}) - (\dot{E}^{TO}_{3b} + \dot{E}^{PH}_{2b})$
MEM	$\dot{E}^{PH}_{10} - (\dot{E}^{PH}_{11} + \dot{E}^{PH}_{12})$	$\dot{E}^{CH}_{11} + \dot{E}^{CH}_{12} - \dot{E}^{CH}_{10}$	–

[a] The stream numbers given here are based on Fig. 3 but might be different from design A to D. For the specific designs, refer the stream numbers according to Figs. S2–S5.
[b] The definitions of the SOE depends on the operating point. For exothermic operation (the case for this paper), the physical-exergy increase between inlet and outlet is counted as co-product, while for endothermic operation, the physical-exergy decrease between inlet and outlet will be counted as exergy fuel.

Results and discussion

Following the flow diagram (Figs. S2–S5), stream data and heat-exchanger information (Tables S1–S8) as well as the definition of exergy fuel, product and co-product (Tables 2 and 3), the system performance and the key terms for exergy evaluation at the component and overall-system levels of all designs are given in Tables S9–S12 and discussed comparatively.

Overall system performance

Heat source for steam generation

As shown in Table 4, if steam utilization of the SOE is over around 60%, it is possible to generate all steam without electrical heating but only by the heat available from the system itself. For all conceptual designs selected, the anode outlet, after preheating the cold sweep gas, can still provide enough heat to generate around 15–18% of the total steam required. Designs A, B and C do not need external electrical steam generator, while design D has over 20% of total steam generated electrically.

Key indicators of system performance

Key indicators of system performances are shown in Table 5. The major power consumption comes from the SOE with a contribution over 95% for designs A, B and C. The system efficiencies of the designs A, B and C with HENs are similar to those of the corresponding conceptual designs (Fig. 4a), for which the required steam can be fully generated by the methanator and anode outlet. Considering the current density preferred by the SOE industry for stack testing, the overall system efficiency (HHV) of PtM can reach over 80% and even 85% with an SOE inlet temperature of 700 °C. However, for the optimal conceptual design D with a low utilization factor of only 55%, the available heat from methanator and anode outlet becomes not sufficient to generate all steam, thus the heat from compression above 100 °C is used for steam generation at around 1 bar, which is hardly practical. Therefore, the heat from compression is replaced by electrical heating of over 0.5 kW (Fig. 4b) for a practical HEN of design D, which results in a significant efficiency decrease of 5 percentage points. In addition, the designs A and B require slight electrical heating to heat cathode inlet to 700 °C, due to less heat available from cathode outlet caused by less heat capacity and low operating voltage (overpotential).

The exergy efficiencies of all designs are close to their energy efficiency based on LHV, around 5% points smaller than those of HHV. The exergy efficiency of the proposed PtM can

Table 4 – Contribution (%) of each steam generator to total steam requirement.

Designs	A	B	C	D
UF	80%	78%	62%	55%
MSG	85	83	82	60
ASSG	15	17	18	17
ELSG	0	0	0	23

Table 5 – Key system performance indicators.

Design	A	B	C	D
p, bar	26	9.7	1.1	1.1
$T_{in,SOE}$, °C	700	700	700	700
$T_{out,SOE}$, °C	746	700	821	821
Steam generation temp., °C	231	184	110	110
Cell voltage, V	1.30	1.32	1.36	1.42
Current density, A/cm^2	0.34	0.61	0.86	0.98
UF, %	80	78	62	55
$\dot{W}_{TOT}$, W	2362	4232	6255	8004
$\dot{W}_{SOE}$, W	2286	4138	5985	7099
$\dot{W}_{ELSH}$, W	35.8	18.6	–	–
$\dot{W}_{ELSG}$, W	–	–	–	531.3
Synthesis natural gas, kg/h	0.1338	0.2380	0.3346	0.3815
Methane, kg/h	0.1306	0.2323	0.3264	0.3721
Energy stored (HHV)[a], W	2013	3581	5033	5737
Energy stored (LHV)[a], W	1858	3305	4647	5298
Energy efficiency (HHV), %	85.2	84.6	80.5	71.7
Energy efficiency (LHV), %	78.7	78.1	74.3	66.2
Exergy efficiency, %	79.4	78.9	75.0	66.9

[a] Only the energy stored by methane with HHV 55.5 MJ/kg and LHV 50 MJ/kg.

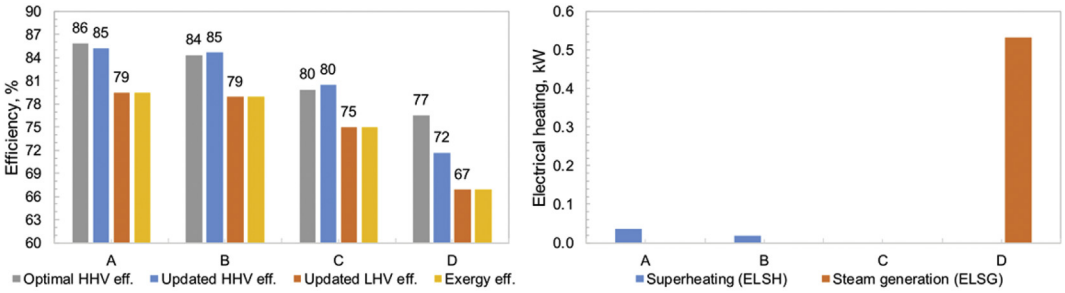

(a) Efficiency comparison (b) Distribution of electrical heating

Fig. 4 – Comparison among the optimal conceptual designs (original designs) and the designs with heat exchanger network (updated designs).

reach between 75% and 80% ($T_{in,SOE} = 700°C$), when the steam utilization is over 60% (designs A, B and C). With a steam utilization below 60%, the system's exergy efficiency can drop significantly below 70%.

Distribution of exergy dissipation

Exergy dissipation by physical processes

The exergy dissipation (destruction and losses) is independent from the definitions of exergy fuel and product. The exergy destruction of each component is grouped based on their physical processes, as shown in Table 6 and Fig. 5). When the UF is over 60%, the exergy destruction variations from design A to B and B to C are consistent with each other. The total exergy destruction is mainly caused by electrochemical and chemical reactions (both between 25 and 35%), followed by heat transfer process (10–17%). The mixing, compression and pumping processes contribute minorly, below 7%. Note that the exergy destruction caused by the reactions also includes the integrated heat transfer process, e.g., internal steam generation for the methanator; therefore, the contribution of heat transfer process should be higher than the number given here. The exergy losses seem quite significant, between 10 and 25%, which offers the opportunity of combined heat and fuel production.

Table 6 – Exergy dissipation caused by physical processes for the four designs (W).

Design	A	B	C	D
UF	80%	78%	62%	55%
Heat transfer[a]	57.57	101	271.3	869.2
Chemical reaction[b]	147.1	272	467	522
Electrochemical reaction[b]	127.0	269	548	724
Mixing	35.38	70.1	105.9	152.3
Compression & pumping	12.18	23.65	77.50	104.3
Loss	126.9	196.6	171.0	394.6

[a] Not including MSG.
[b] Including the heat transfer inside the components where the processes occur.

For designs A, B and C with the UF over 60%, an increase in current density (methane yield) leads to an increase in the exergy-destruction contribution from the SOE, from 25% for the design A to 30% for B and 33% for C. This is mainly due to the increased overpotential, an indicator for the irreversibility of electrochemical processes. The contribution of the chemical reaction keeps almost constant of 30%. The contribution of heat transfer for designs A and B is similar, but an increase of 5 percentage points from design B to C is observed. The contributions of exergy losses from design A to C are reduced significantly from 25% to 10%.

Compared with designs A, B and C, the design D with low steam utilization in SOE and large electrical steam generation shows very different distribution. From the design C to D, the significant increase in the contribution of heat transfer processes, almost doubled from 17% (C) to 31% (D), largely reduces those of all other processes, 19% and 26% from chemical and electrochemical reactions.

Exergy destruction by components

The exergy-destruction contribution from the SOE and RMETH has been given above. The destruction of each heat exchanger to the total heat-transfer exergy destruction (not including MSG) is compared in Fig. 6a. For the designs A – C, major exergy destructions come from PMSG (20–35%), ASSG (25–50%) and AAHE (>30%, if exists). The share of FFHE remains stable at around 13–20%. ELSH can contribute up to 20% to the total heat-transfer exergy destruction. The design D shows quite different picture: The ELSG solely contributes 50%, followed by AAHE (around 30%). Due to large contribution of ELSG, the shares of all other heat exchangers are largely reduced, compared with those of designs A – C.

The exergy-destruction contribution (Fig. 6a) differs significantly from the heat-load share (Fig. 6b): (1) The heat-load shares of ASSG and PMSG are similar for designs A and B. However, ASSG's exergy-destruction share of design B is significantly higher than that of A and PMSG's contribution of design B becomes lower than that of A. The former is mainly caused by an increased heat-transfer temperature difference (HTTD), due to an increased inlet temperature of the hot sweep air (746 and 819 °C for A and B) and a reduced temperature for steam generation (231 and 184 °C for A and B). The

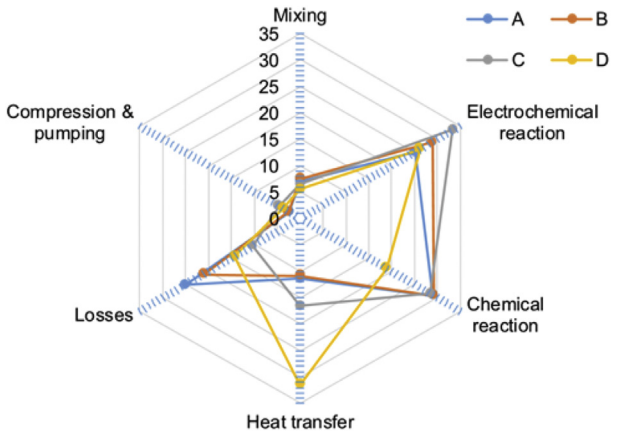

Fig. 5 – Contribution of each process to exergy dissipation (%).

increased share of ASSG reduces PMSG's contribution, although the HTTD of PMSG is also increased limitedly due to the decrease in steam-generation temperature. (2) The exergy-destruction ratio of FFHE follows that of the heat-load share, since its HTTD of design B – D is similar to each other. (3) Electrical heating is limited due to plant-wise heat integration, but its exergy destruction is significant, particularly when electricity is used to generate steam at around 100 °C (design D), which completely change the picture of design D. Reducing electrical heating is crucial for improving the system performance, and particularly, electrical steam generator should be avoided.

Exergy losses and co-generation opportunity

The share of exergy losses is reduced slightly from design A to C, from 25 to 10% of total exergy dissipation. The losses of design C (197 W) is even lower than that of design B (171 W). The losses are mainly contributed by the exhausts of FFHE, AASG and PMSG, over 85%. As shown in Fig. 7, the losses may be recovered mainly from the thermal exergy of FFHE and AASG exhausts, which contribute about 35–40% and 25–30% to the total exergy losses. Particularly, for the design C, the share of thermal exergy loss from the FFHE exhaust reaches over 50%. Considering that the temperature levels of the exhaust gases are all over 100 °C, even above 150 °C up to 200 °C for the design A and B, there is quite big opportunity of utilizing the available thermal exergy for district heating. One may mention that the thermal exergy from the FFHE exhaust can also support certain steam generation; however, the amount is limited due to the low heat capacity of hydrogen-rich flow and it is not wise to introduce a small steam generator considering the system complexity. In addition, further considering the chemical exergy of the O_2 available in sweep-gas exhaust, particularly of designs A and B, even a higher co-generation opportunity is possible: around 45% from the FFHE exhaust and over 40% from the AASG exhaust.

Exergy efficiency of each component

The exergy efficiency of each component calculated based on different definition approaches has been shown in Tables S9–S12 for all four designs, respectively.

Comparison between productive and thermodynamic efficiencies

For the components used in the PtM system, the co-products are mainly related to the compressor, chemical and electrochemical reactors. The evaluation of co-products for multi-stage compressors is not performed, since it requires detailed information of the outlet streams of each stage. However, this does not affect the value of exergy efficiency significantly, as the temperature of gas flows after compression is usually slightly above 100 °C considering a maximum pressure ratio of 4 and the thermal exergy is limited. The co-products for RMETH and SOE have been described in Implementation.

It can be seen from Tables S9–S12 that, for all the four designs, there is no big difference between the productive and thermodynamic exergy efficiencies for both the TMNR and PC approaches. The difference is slightly increased from the design A (average 0.5 percentage point) to D (average 2

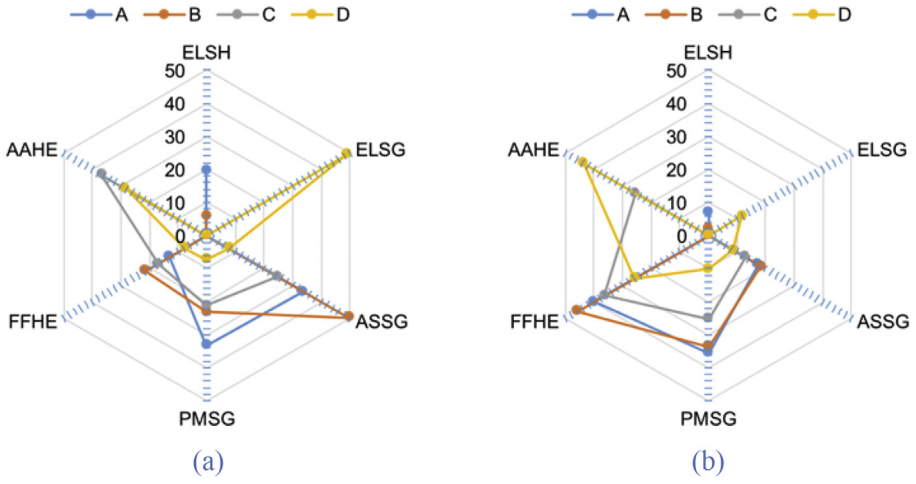

Fig. 6 – Contribution (%) of exergy destruction (a) and load (b) of heat exchangers to the total number of heat transfer process (not including MSG).

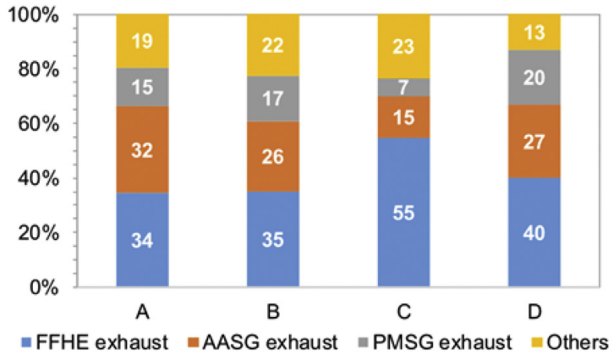

Fig. 7 – Share of thermal exergy losses from the exhausts of heat exchangers (%).

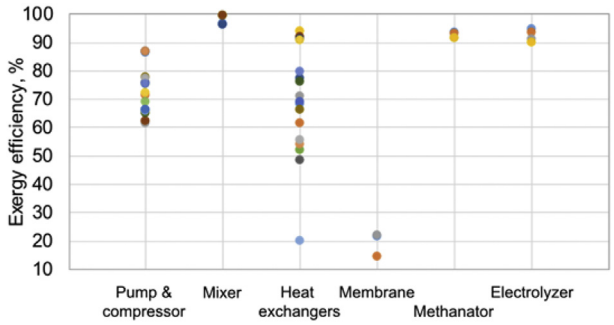

Fig. 8 – Exergy efficiency of all components.

percentage points). Particularly, for the SOE of design D, the difference reaches the highest, 3.5–4 percentage points. This is mainly due to the increased feed flowrates of the reactant and sweep air, which lead to much more heat carried out of the SOE. Also, for design D, the increased oxygen product further increases exergy co-product of SOE.

For the RMETH, the difference between productive and thermodynamic efficiencies remains stable below 1 percentage point, since the inlet and outlet temperatures of the gas mixtures are similar among four designs and the flowrates are also proportional to the inlet H_2. In such a case, the thermal exergy carried away by the gas mixtures remains limited, compared to the converted by chemical reaction and transferred for steam generation.

Comparison among three definition approaches of exergy efficiency

The exergy efficiencies calculated based on the IO approach are all quite high over 80%, mostly over 95%, except that of the electrical steam generator, ELSG, of the design D due to the low exergy content of its water inlet. Thus, there is a lack of discrimination by using IO exergy efficiency to evaluate the thermodynamic perfection of most components. The IO approach should be avoided for component-based exergy evaluation.

The discrimination of exergy efficiencies calculated by the TMNR and PC are from SOE, MEM and RMETH. For SOE and MEM, the two approaches are approximately equivalent with a difference below 0.5 percentage point. For the SOE, the TMNR definition shifts a small amount of exergy product from that defined by PC. However, given the large exergy fuel, the electricity consumption, the effect of the shift is very limited.

For the RMETH, the differences between the TMNR and PC approaches are much larger and can reach even as high as 4.5 percentage points for the design D. With TMNR, the exergy fuel can be accurately defined as the chemical exergies of H_2 and CO_2, which is lower than that of the PC, the total chemical exergy of the reactor inlet gas. For the PC approach, the chemical exergies not related to the H_2, CO_2 and CH_4 are added to both the exergy fuel and product, which increases the efficiency number. Given this comparison, we encourage to use the TMNR approach to evaluate the system with chemical reactions involved.

TMNR exergy efficiency of each component

Given the difference described in Comparison between productive and thermodynamic efficiencies and Comparison among three definition approaches of exergy efficiency, we discuss below only the thermodynamic exergy difference calculated by the TMNR approach, as shown in Fig. 8. The exergy efficiencies of pumps (85–90%) are higher than those of the compressors (60–80%), which depends on the type of gas (mixture) compressed and the isentropic efficiency. The mixers are with very high exergy efficiency of over 95%, since the mixing processes involved occur with similar incoming temperatures. The variation of the efficiencies of heat exchangers is large, mostly between 50 and 80%. For the electrical heaters, the ELSG works with the lowest efficiency of 20%, due to large irreversibility of converting electricity to heat around 100 °C. The irreversibility is reduced by electricity-to-heat at over 600 °C with an exergy efficiency of 70% for ELSH. For other heat exchangers, the exergy efficiency depends on two factors: the temperature level of the cold stream and HTTD. The higher the temperature level of the cold stream, the higher the exergy efficiency will be [29]. This is mainly the reason of an efficiency over 90% for FFHE The ASSG suffers from both relatively low temperature level of the cold stream and high HTTD, leading to an efficiency between 50 and 60%. The PMSG has relatively small HTTD and achieves an efficiency mostly above 65%. The membrane efficiency is below 20%, indicating that using mechanical exergy to separate the non-reactive chemical exergy is not a good choice although membrane separation can be less energy-intensive than other technologies. The RMETH's exergy efficiency is above 90% due to effective extraction of reaction heat via steam generation and high conversion rate, which helps to convert most of the reactive chemical exergy of H_2 and CO_2 to CH_4 but not to the thermal exergy of the outlet gas. The SOE's exergy efficiency is also high between 89 and 93%, since the input electricity is mostly converted to the chemical exergy but not heat, and the thermal exergy increase from the SOE inlet to outlet is limited due to the constraint of a maximum temperature difference of 120 °C. In addition, the efficiency of SOE decreases from design A to D, due to the increased overpotential (electricity converted to heat).

Conclusions

In this paper, we derived and evaluated four SOE-based PtM plant designs with specific HENs via a top-down approach considering step-by-step the system concept, optimal conceptual designs, design-point selection and HEN design. The heat sources for steam generation, the key to realize high system efficiency of such PtM plants, are identified from the HEN design. Then, the four system designs are evaluated with exergy analysis and TMNR exergy system to identify the exergy dissipation within the system and exergetic performance of each component. The major conclusions include:

- The operating point of the SOE, particularly the steam utilization factor, determines how the steam generation will be supported by the heat available inside the system. For the analyzed systems, when the steam utilization is over 60%, all steam can be generated without electrical heating with around 80–85% by methanation heat and 15–18% by the heat from anode outlet.
- The system efficiency with a SOE inlet temperature of 700 °C can reach as high as 80–85% (HHV) and 75–80% (LHV), similar to the exergy efficiency. Introducing electrical steam generation when the UF is over 60% will significantly reduce the system efficiency below 70% (LHV).
- The overall exergy dissipation is mostly contributed by the SOE (25–35%), RMETH (25–35%) and heat exchangers (15–18%, not including MSG) and losses (10–25%). The exergy destruction of the heat exchangers mainly occurs in PMSG (20–35%), ASSG (25–50%) and AAHE (>30%, if used). ELSG, if applied, will contributes significant amount of exergy destruction.
- Exergy losses are mainly caused by the thermal exergy of the cathode and anode exhausts, about 35–40% and 25–30%. The exhaust temperatures can be over 200 °C and mostly over 100 °C, which offers the opportunity of co-generation for space heating.
- The TMNR definition for exergy efficiency of each component is more accurate for chemical reactors; however, PC definition is already adequate for the PtM plants. The IO approach should be avoided. The exergy efficiencies are 60–80% for compressors, 50–90% for heat exchangers, over 90% for RMETH and SOE. The ELSG and MEM have only an efficiency around 20%.
- Considering the impact on the system efficiency, the primary design target for such systems should be no use of electrical steam generation. Small amount of electrical heating to heat SOE inlet to the desired temperature, however, is acceptable.

Acknowledgments

The research leading to these results has received funding from the European Union's Horizon 2020 (H2020-LCE-2016-2017) for the Competitive Low-carbon Energy under grant agreement n° 731125, PENTAGON.

Appendix A. Supplementary data

Supplementary data to this article can be found online at https://doi.org/10.1016/j.ijhydene.2018.11.151.

Nomenclatures

Abbreviations

AAHE	air-air heat exchanger
AASG	air-side steam generator
CP	compressor & pump
ELSG	electrical steam generator
ELSH	electrical superheater
FD	flash drum
FFHE	fuel-fuel heat exchanger
HEN	heat exchanger network
HHV	higher heating value
HTTD	heat-transfer temperature difference
LHV	lower heating value
IO	input-output
MEM	membrane
MSG	main steam generator
MX	mixer
PC	physical-chemical
PMSG	preheater of main steam generator
PtG	power-to-X
PtM	power-to-methane
PtX	power-to-gas
RES	renewable energy source
RMETH	methanation reactor
SNG	synthesis natural gas
SP	splitter
SOE	solid-oxide electrolyzer
TMNR	thermal – mechanical – non-reactive – reactive
UF	utilization factor
VRES	variable renewable energy sources

Mathematical symbols

$\bar{e}$	standard chemical exergy
E	specific exergy
$\dot{E}$	exergy flow
$\dot{F}$	molar flow rate
H	specific enthalpy
J	current density
n	molar flowrate
R	gas constant
T	temperature
p	pressure
S	specific entropy
V	voltage
$\dot{W}$	power
x	molar composition
y	molar composition
ϵ	exergy efficiency
η	energy efficiency

Subscripts

0	reference

C	co-product
D	destruction
f	
F	fuel
stm	steam
METH	methanator or methanation
P	product
PERM	permeate flow
SYS	system

Superscripts

i, j, k	index
CH	chemical
l	liquid
g	gas
ME	mechanical
N	non-reactive
P	productive
PH	physical
R	reactive
T	thermodynamic
TH	thermal
TO	total

REFERENCES

[1] Carley S, Baldwin E, MacLean LM, Brass JN. Global expansion of renewable energy generation: an analysis of policy instruments. Environ Resour Econ 2017;68:397–440.

[2] Lacal Arantegui R, Jäger-Waldau A. Photovoltaics and wind status in the European Union after the Paris agreement. Renew Sustain Energy Rev 2018;81:2460–71. https://doi.org/10.1016/j.rser.2017.06.052.

[3] Eurostat. Share of energy from renewable sources. 2018. Last update: 08-03-2018, http://appsso.eurostat.ec.europa.eu/nui/submitViewTableAction.do. [Accessed 26 March 2018].

[4] Warner KJ, Jones GA. The climate-independent need for renewable energy in the 21st century. Energies 2017;10(8):1197. https://doi.org/10.3390/en10081197.

[5] Yao E, Wang H, Wang L, Xi G, Maréchal F. Thermo-economic optimization of a combined cooling, heating and power system based on small-scale compressed air energy storage. Energy Convers Manag 2016;118:377–86.

[6] Yao E, Wang H, Wang L, Xi G, Maréchal F. Multi-objective optimization and exergoeconomic analysis of a combined cooling, heating and power based compressed air energy storage system. Energy Convers Manag 2017;138:199–209.

[7] Kondziella H, Bruckner T. Flexibility requirements of renewable energy based electricity systems – a review of research results and methodologies. Renew Sustain Energy Rev 2016;53:10–22. https://doi.org/10.1016/j.rser.2015.07.199.

[8] McPherson M, Tahseen S. Deploying storage assets to facilitate variable renewable energy integration: the impacts of grid flexibility, renewable penetration, and market structure. Energy 2018;145:856–70. https://doi.org/10.1016/j.energy.2018.01.002.

[9] Blanco H, Faaij A. A review at the role of storage in energy systems with a focus on power to gas and long-term storage. Renew Sustain Energy Rev 2018;81:1049–86. https://doi.org/10.1016/j.rser.2017.07.062.

[10] Mennicken L, Janz A, Roth S. The German R&D program for CO2 utilization – innovations for a green economy. Environ Sci Pollut Res 2016;23:11386–92. https://doi.org/10.1007/s11356-016-6641-1.

[11] Zinck Thellufsen J, Lund H. Cross-border versus cross-sector interconnectivity in renewable energy systems. Energy 2017;124:492–501. https://doi.org/10.1016/j.energy.2017.02.112.

[12] Ghaib K, Ben-Fares F-Z. Power-to-methane: a state-of-the-art review. Renew Sustain Energy Rev 2018;81:433–46. https://doi.org/10.1016/j.rser.2017.08.004.

[13] Sıdkı Uyar T, Beşikci D. Integration of hydrogen energy systems into renewable energy systems for better design of 100% renewable energy communities. Int J Hydrogen Energy 2017;42:2453–6. https://doi.org/10.1016/j.ijhydene.2016.09.086.

[14] Engerer H, Horn M. Natural gas vehicles: an option for Europe. Energy Pol 2010;38:1017–29. https://doi.org/10.1016/j.enpol.2009.10.054.

[15] Lehner M, Tichler R, Steinmüller H, Koppe M. Power-to-gas: technology and business models. [Chapter 2]: the power-to-gas concept. 2014. p. 7–17. https://doi.org/10.1007/978-3-319-03995-4_2. ISBN: 978-3-319-03994-7.

[16] Kopp M, Coleman D, Stiller C, Scheffer K, Aichinger J, Scheppat B. Energiepark Mainz: technical and economic analysis of the worldwide largest power-to-gas plant with PEM electrolysis. Int J Hydrogen Energy 2017;42:13311–20. https://doi.org/10.1016/j.ijhydene.2016.12.145.

[17] Ludwig M, Haberstroh C, Hesse U. Exergy and cost analyses of hydrogen-based energy storage pathways for residual load management. Int J Hydrogen Energy 2015;40:11348–55. https://doi.org/10.1016/j.ijhydene.2015.03.018.

[18] Foit SR, Vinke IC, de Haart LGJ, Eichel R-A. Power-to-syngas: an enabling technology for the transition of the energy system? Angew Chem 2016;129(20). https://doi.org/10.1002/ange.201607552.

[19] HELMETH. European Union's seventh framework programme (fp7/2007-2013) for the fuel cells and hydrogen joint technology initiative: integrated high-temperature electrolysis and methanation for effective power to gas conversion. http://www.helmeth.eu/. [Accessed 26 March 2018].

[20] Founti M. Power-to-gas concept and overview of helmeth project. NTUA dissemination event: energy storage technologies: focus on power-to-gas technology. 2016.

[21] Karlsruhe Institute of Technology. Power-to-gas facility with high efficiency. 2018. https://phys.org/news/2018-03-power-to-gas-facility-high-efficiency.html. [Accessed 26 March 2018].

[22] Luo Y, Wu X, Shi Y, Ghoniem AF, Cai N. Exergy analysis of an integrated solid oxide electrolysis cell-methanation reactor for renewable energy storage. Appl Energy 2018;215:371–83.

[23] www.etip-snet.eu/wp-content/uploads/2017/06/2.-John-B%C3%B8gild-HANSEN-The-El-upgraded-biogas-Project.pdf.

[24] www.pentagon-project.eu/.

[25] Wang L, Pérez-Fortes M, Madi H, Diethelm S, Van herle J, Maréchal F. Optimal design of solid-oxide electrolyzer based power-to-methane systems: a comprehensive comparison between steam electrolysis and co-electrolysis. Appl Energy 2018;211:1060–79. https://doi.org/10.1016/j.apenergy.2017.11.050.

[26] Wang L, Mian A, de Sousa LC, Diethelm S, Van herle J. Integrated system design of a small-scale power-to-methane demonstrator. Chem Eng.Trans 2017;61:1339–44.

[27] Wang L. Thermo-economic evaluation, optimization and synthesis of large-scale coal-fired power plants. Doctoral Thesis. Technical University of Berlin; 2016. https://www.depositonce.tu-berlin.de/handle/11303/5852.

[28] Kaushik SC, Siva Reddy V, Tyagi SK. Energy and exergy analyses of thermal power plants: a review. Renew Sustain

Energy Rev 2011;15:1857–72. https://doi.org/10.1016/j.rser.2010.12.007.
[29] Yang Y, Wang L, Dong C, Xu G, Morosuk T, Tsatsaronis G. Comprehensive exergy-based evaluation and parametric study of a coal-fired ultra-supercritical power plant. Appl Energy 2013;112:1087–99.
[30] Wang L, Yang Y, Morosuk T, Tsatsaronis G. Advanced thermodynamic analysis and evaluation of a supercritical power plant. Energies 2012;5(6):1850–63.
[31] Wang L, Yang Y, Dong C, Yang Z, Xu G, Wu L. Exergoeconomic evaluation of a modern ultra-supercritical power plant. Energies 2012;5(9):3381–97.
[32] Ahamed JU, Saidur R, Masjuki HH. A review on exergy analysis of vapor compression refrigeration system. Renew Sustain Energy Rev 2011;15:1593–600. https://doi.org/10.1016/j.rser.2010.11.039.
[33] Aghbashlo M, Mobli H, Rafiee S, Madadlou A. A review on exergy analysis of drying processes and systems. Renew Sustain Energy Rev 2013;22:1–22. https://doi.org/10.1016/j.rser.2013.01.015.
[34] Bayrak F, Abu-Hamdeh N, Alnefaie KA, Öztop HF. A review on exergy analysis of solar electricity production. Renew Sustain Energy Rev 2017;74:755–70.
[35] Kalogirou SA, Karellas S, Braimakis K, Stanciu C, Badescu V. Exergy analysis of solar thermal collectors and processes. Prog Energy Combust Sci 2016;56:106–37.
[36] Im-orb K, Visitdumrongkul N, Saebea D, Patcharavorachot Y, Arpornwichanop A. Flowsheet-based model and exergy analysis of solid oxide electrolysis cells for clean hydrogen production. J Clean Prod 2018;170:1–13. https://doi.org/10.1016/j.jclepro.2017.09.127.
[37] Ni M, Leung MKH, Leung DYC. Energy and exergy analysis of hydrogen production by solid oxide steam electrolyzer plant. Int J Hydrogen Energy 2007;32:4648–60.
[38] Stempien JP, Ding OL, Sun Q, Chan SH. Energy and exergy analysis of Solid Oxide Electrolyser Cell (SOEC) working as a CO2 mitigation device. Int J Hydrogen Energy 2012;37:14518–27. https://doi.org/10.1016/j.ijhydene.2012.07.065.
[39] Bernadet L, Gousseau G, Chatroux A, Laurencin J, Mauvy F, Reytier M. Influence of pressure on solid oxide electrolysis cells investigated by experimental and modeling approach. Int J Hydrogen Energy 2015;40(38):12918–28.
[40] Rinaldi G, Diethelm S, Oveisi E, Burdet P, Van Herle J, Montinaro D, et al. Post-test analysis on a solid oxide cell stack operated for 10,700 hours in steam electrolysis mode. Fuel Cell 2017;17(4):541–9.
[41] Rao M, Sun X, Hagen A. Long term testing of solid oxide electrolysis cells under Co-electrolysis conditions. E C S Trans 2017;80(9):57–69. https://doi.org/10.1149/08009.0057ecst.
[42] Pietsch P. Dynamic modeling and optimal design of small-scale, evaporator-integrated methanator reactor. Master thesis. Germany: Technical University of Darmstadt; 2018.
[43] Basu S, Khan AL, Cano-Odena A, Liu C, Vankelecom IFJ. Membrane-based technologies for biogas separations. Chem Soc Rev 2010;39(2):750–68. https://doi.org/10.1039/B817050A.
[44] Fu P, Wang N, Wang L, Morosuk T, Yang Y, Tsatsaronis G. Performance degradation diagnosis of thermal power plants: a method based on advanced exergy analysis. Energy Convers Manag 2016;130:219–29.
[45] Wang L, Fu P, Wang N, Morosuk T, Yang Y, Tsatsaronis G. Malfunction diagnosis of thermal power plants based on advanced exergy analysis: the case with multiple malfunctions occurring simultaneously. Energy Convers Manag 2017;148:1453–67.
[46] Penkuhn M, Tsatsaronis G. Application of exergy analysis for evaluating chemical reactor concepts. In: Proceedings of ECOS 2018- the 31th International conference on efficiency, cost, optimization, simulation and environmental impact of energy systems; 2018. June 17-22, 2018, Guimaraes, Portugal.
[47] Bejan A, Tsatsaronis G, Moran M. Thermal design and optimization. John Wiley & Sons; 1996.
[48] Szargut J. Exergy method: technical and ecological applications. Developments in heat transfer. WIT Press; 2005. 978-1853127533.
[49] Lazzaretto A, Tsatsaronis G. SPECO: a systematic and general methodology for calculating efficiencies and costs in thermal systems. Energy 2006;31(8–9):1257–89.